Removing autocorrelation in spectral optical coherence tomography

Jun Ai, Lihong V. Wang

Jun Ai, Lihong V. Wang, "Removing autocorrelation in spectral optical coherence tomography," Proc. SPIE 6079, Coherence Domain Optical Methods and Optical Coherence Tomography in Biomedicine X, 60790Z (20 February 2006); doi: 10.1117/12.647817

SPIE.

Event: SPIE BiOS, 2006, San Jose, California, United States

Removing autocorrelation in spectral optical coherence tomography

Jun Ai* and Lihong V. Wang
Optical Imaging Laboratory, Department of Biomedical Engineering, Texas A&M University, 3120 TAMU, College Station, TX 77843-3120

ABSTRACT: We have developed a new algorithm and configuration for removing the autocorrelation of the object wave in spectral optical coherence tomography. The self-interferogram of the object wave is acquired synchronously with the standard interferogram of the recombined object and reference waves. The former is then subtracted from the latter after Fourier transformation. The algorithm is validated by numerical simulation and by experimental measurement of a USAF target and a feline eye.
Keywords: optical coherence tomography, medical optics instrumentation, optical diagnostics for medicine

Spectral optical coherence tomography or Fourier domain optical coherence tomography (FDOCT) has drawn significant attention recently.[1-5] FDOCT has been shown to offer faster A-scan speed and higher sensitivity than time-domain optical coherence tomography (TDOCT).[6-7] A readout rate of 29 kHz in a line-scan CCD camera provides an A-scan rate equivalent to hundreds of meters per second,[3] which easily surpasses the grating-lens-based rapid scanning optical delay line (RSOD) that is widely used in high-speed TDOCT.

The main challenges to developing high-performance FDOCT are the autocorrelation (AK) interference and ghost images, both of which obscure the interpretation of images and degrade the system sensitivity. To tackle these problems, some investigators have developed full-range complex FDOCT to construct the complex field of the object wave by retrieving the phase information, which is accomplished by modulating the phase delay in the reference arm through a phase modulator or a piezo-actuator.[3-5] A common problem with the phase shifting technique, however, is the polychromatic phase error, i.e., the dependence of phase shift on wavelength, which may introduce significant phase errors in ultra-high resolution FDOCT where the bandwidth of the source is >100 nm. Other potential issues include the repeatability and stability of piezo-actuation, and higher-order dispersion introduced by electro-optical crystal in the phase modulator. The AK self-elimination technique we present below is tasked to eradicate all of these problems.

The standard interferogram $ro(k)$ acquired by a typical Michelson interferometer-based FDOCT can be expressed as

$$ro(k) = \left|E_o(k) + E_r(k)\right|^2 , \tag{1}$$

where $k = 2\pi / \lambda$ is the wave-number with λ being the wavelength in vacuum; $E_o(k)$ and $E_r(k)$ are the back-scattered optical fields from the object and the reference mirror, respectively. Eq. (1) can be expanded and rearranged to

$$xc(k) = ro(k) - obj(k) - ref(k) , \tag{2}$$

where $xc(k) = 2\,\mathrm{Re}[E_o(k)E_r(k)^*]$ is the mutual interference between the object and the reference waves; $obj(k) = |E_o(k)|^2$ is the self-interferogram of the object wave; and $ref(k) = |E_r(k)|^2 = s(k)$ is the spectral intensity of the source. The space domain counterpart of Eq. (2) is then obtained:

$$XC(z) = RO(z) - OBJ(z) - REF(z), \tag{3}$$

*Dr. Jun Ai is currently with Luminit, LLC, a new spin-off from Physical Optics Corporation, Torrance, CA 90501.

Coherence Domain Optical Methods and Optical Coherence Tomography in Biomedicine X
edited by Valery V. Tuchin, Joseph A. Izatt, James G. Fujimoto, Proc. of SPIE Vol. 6079
60790Z, (2006) · 1605-7422/06/$15 · doi: 10.1117/12.647817

where *OBJ(z), RO(z)* and *REF(z)* are the inverse Fourier transforms of *obj(k), ro(k)* and *ref(k)*, respectively. *XC(z)* is the cross-correlation between the object and the reference waves, which gives the profile of the normalized amplitude reflection coefficient of the object and, therefore, is the signal we need to extract. *OBJ(z)* is the AK of the object wave and contains not only a DC component (located at $z = 0$) but also the AC components (located at $z \neq 0$) that are mixed with *XC(z)*.

Our algorithm requires that one first acquire $ro(k)$, $obj(k)$ and $ref(k)$ and then Fourier transform them to *RO(z), OBJ(z),* and *REF(z).* The *XC(z)* is obtained simply by subtracting *OBJ(z)* and *REF(z)* from *RO(z)*. This is why we call the algorithm "the self-elimination of AK interference," or **SEA** in short. $ref(k)$ needs to be acquired only once by blocking the object arm for the entire image, whereas $ro(k)$ and $obj(k)$ have to be acquired for each A-scan. The subtraction of $REF(z)$ is necessary if the source is not perfectly Gaussian or if there are ripples in the spectrum $ref(k)$. Keep in mind that the Fourier transformation from Eq. (2) to Eq. (3) requires uniform sampling in wave-number. In a spectrometer, however, the spectrum is evenly spread in wavelength. Therefore, the raw spectrum must be interpolated to avoid degrading the axial resolution and SNR[8].

Note that *XC(z)* contains two parts: the object itself and the ghost (mirror) of the object. The ghost may overlap with the object if the reference plane is placed improperly. By placing the reference plane outside of the object (or the region of interest), the ghost is shifted to the other side of the object and, therefore, can be removed by retaining only the positive AC components. The sacrifice is that the measurement range is reduced by half compared with full-range complex FDOCT.

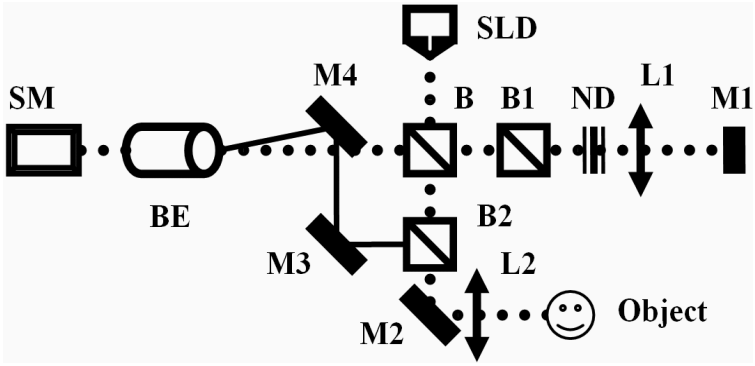

Figure 1. Schematic of a SEA FDOCT system. SLD: super-luminescent diode; B, B1 and B2: beam splitters; L1-L2: lenses; BE: beam expander; ND: neutral density filter; M1-M4: mirrors; SM: spectrometer.

A schematic diagram of a SEA FDOCT system is shown in Fig. 1. The 1.6-mW collimated light from an SLD source at 850 nm with a FWHM of 23 nm is split into reference and object arms by a beam splitter B. The maximum power delivered to the object is 0.3 mW. The B-scan is provided by a galvanometer mirror M2 (Cambridge 6220M). The back-scattered waves from the object and the reference mirror M1 are expanded by beam

expander BE before reaching a spectrometer comprising a diffraction grating G (Wasatch Photonics 1200 lp/mm Volume Phase Holographic Transmission Grating for 850 nm), an achromatic (focal length 400 mm), and a CCD camera (Andor 16-bit 1024x256 array, pixel 26 micron square). The backscattered light of the object (the solid line) is sampled by beam splitter B2, redirected by mirror M3, and then imaged to different row(s) in the CCD array by tilting mirror M4, which is placed just above the recombined light exiting from beam splitter B. Since $ro(\lambda)$ and $obj(\lambda)$ are simultaneously recorded by the CCD array (in different rows), synchronous elimination of AK is achieved. To compensate for the dispersion introduced by beam splitter B2 in the object arm, an identical beam splitter B1 is placed in the reference arm. The data acquisition of the CCD camera is externally triggered and synchronized with the B-scan signal by a custom-developed LabVeiw program. The spectrometer is able to measure a wavelength range of 47.7 nm with a spectral resolution of $\delta\lambda = 46.6\,pm$ at $\lambda_0 = 850\,nm$, which translates to an FDOCT measurement range of $z_{\max} = 3.9\,mm$ in the air according to $z_{\max} = \lambda_0^2/(4\delta\lambda)$. The measured sensitivity is 112 dB at 0.3 mm, and it gradually reduces to 100 dB at 3.7 mm. The decrease in sensitivity with depth is caused by the finite spectral resolution of the spectrometer.[2] The measured axial resolution is 15 μm in air.

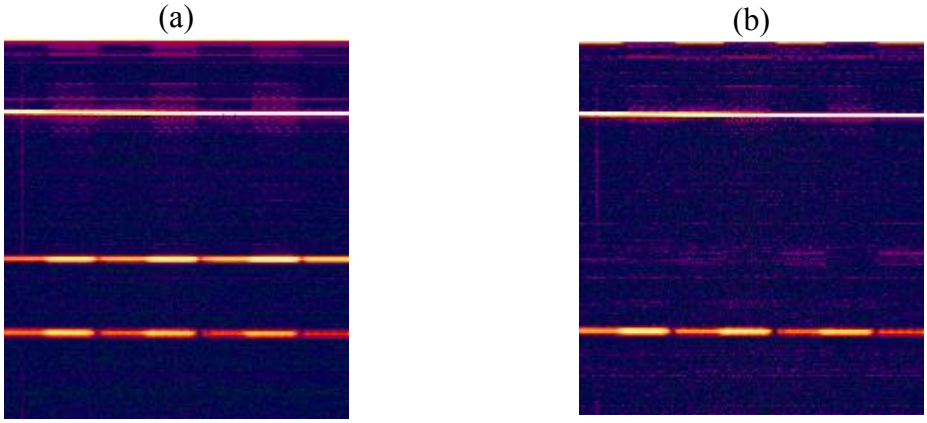

Figure 2. FDOCT images of a USAF 1951 target (a) before, and (b) after self-elimination of AK. B-scan from left to right 1.95 mm across the "III" bar pattern in group 0, element 6. A-scan from top to bottom 3.9 mm in air.

To validate the capability of AK self-elimination of our FDOCT system, a USAF 1951 positive target is imaged. The B-scan is performed across the "III" bar pattern and consists of 200 exposures, acquired in 4 seconds. Each exposure records both $ro(\lambda)$ and $obj(\lambda)$ in two separate tracks, each track comprising 4 rows vertically binned to 1024 pixels. The raw spectra $ro(\lambda)$ is interpolated to the k-domain and then Fourier transformed to $RO(z)$, which is shown in Fig. 2 (a), where the reference plane is at the top (z = 0). The 1st bright line down at z = 0.771 mm is the 1st surface of the target and the 3rd line is the 2nd surface. The optical spacing between them is 2.259 mm, which agrees with the specified thickness (1.5 mm) of the target assuming a refractive index of 1.5. The 2nd line is the AK between the two surfaces and is located at z = 2.259 mm, which also agrees with the thickness of

the target. The lateral B-scan crosses 3.5 line pairs in group 0, element 6 and covers 1.95 mm on the target, which agrees with the specified spatial resolution of 1.78 lp/mm. Likewise, $obj(\lambda)$ is Fourier transformed to $OBJ(z)$, which is then subtracted from $RO(z)$ to extract the two surfaces of the target, as shown in Fig. 2(b).

Figure 3(a) is a measured *ex vivo* image of a feline eye. The reference plane is placed 0.213 mm before the front surface of the cornea. The AK of the object is clearly seen from z = 0 to 1 mm in the cornea. The thick bright line at z = 2.2 mm is caused by ripples in the source spectrum, which were introduced intentionally to test the functionality of source AK self-elimination. Figure 3(b) is the image after AK self-elimination. It is clear that the object AK and the side lobes of the source are removed completely.

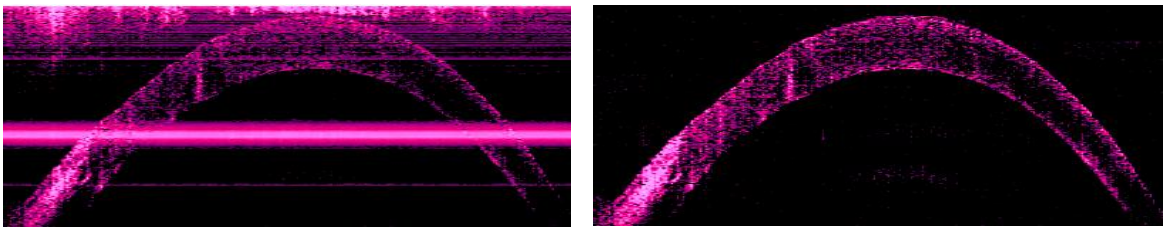

(a) (b)

Figure 3. FDOCT images of a feline eye (a) before, and (b) after AK self-elimination. A-scan from top to bottom 3.9 mm in air, B-scan from left to right 15 mm.

We have developed a program to simulate the AK self-elimination. The simulated object is a glass slide of 1 mm thick. The refractive index is assumed to be 1.5. Figure 4 (a) and (b) show the simulated $ro(\lambda)$ and $obj(\lambda)$ of the glass. The $ro(\lambda)$ is then interpolated and Fourier transformed to $RO(z)$, which is shown in Fig. 4(c) where the reference plane is at z = 0. The amplitude of the DC component is 14758 and is truncated at 6000 in order to show the smaller AC peak (amplitude 4226.4) at z = 1.5 mm. The two peaks at z = 1.0 mm and 2.5 mm correspond to the two surfaces of the glass, where the spacing between them agrees with the thickness of the glass. Likewise, $obj(\lambda)$ is Fourier transformed to $OBJ(z)$, which consists of two peaks: a DC with amplitude 9705.1, and an AC at z = 1.5 mm with amplitude 4226.3, as shown in Fig. 4(c). The location of the AC peak also agrees with the thickness of the glass. $REF(z)$ is also calculated and appears as a DC peak with amplitude 5050.7, which, if added with the DC peak of $OBJ(z)$, agrees well with the DC amplitude of $RO(z)$. The $XC(z)$ shown in Fig. 4(d) is obtained by subtracting $OBJ(z)$ and $REF(z)$ from $RO(z)$. It is clear that the AK of both the glass and the source is completely removed.

In conclusion, we have developed a self-elimination algorithm of AK interference and built a FDOCT system capable of synchronous AK self-elimination. The algorithm is validated by numerical simulation and experimental measurement of a USAF target and a feline eye.

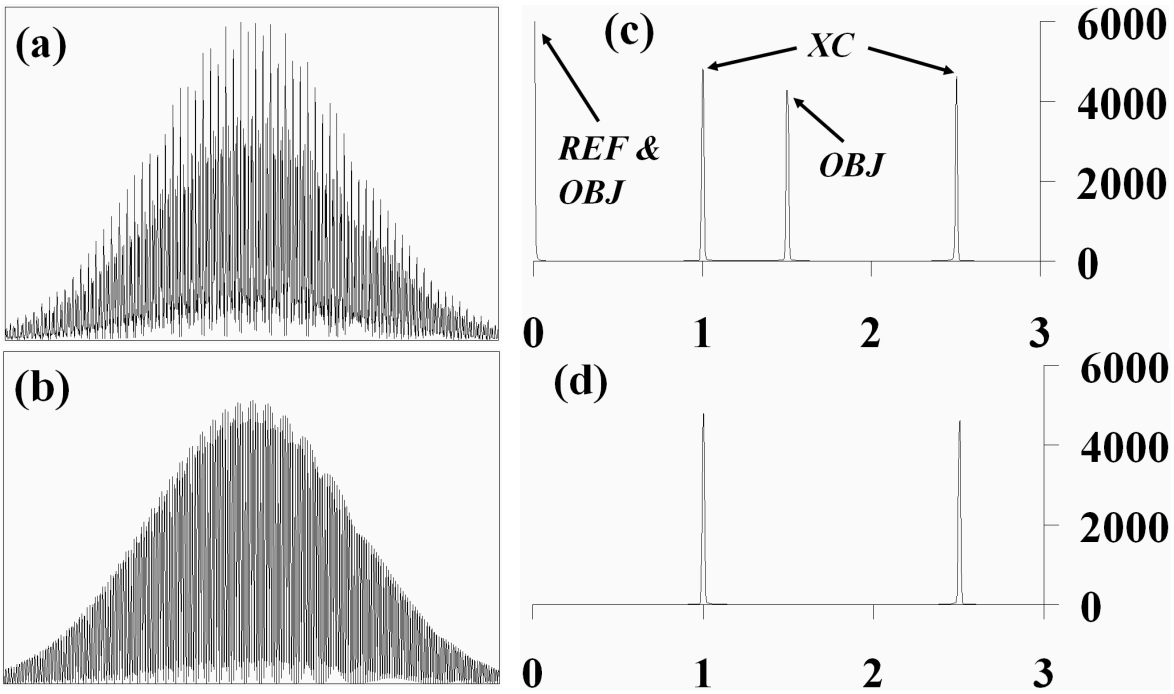

Figure 4. Simulated (a) $ro(\lambda)$, (b) $obj(\lambda)$, (c) *RO(z)*, and (d) *XC(z)* of a glass slide. The vertical scale of (b) is half of (a). The *x* and *y* axes in (c) and (d) are optical depth (mm) and amplitude, respectively.

We thank Dr. George Stoica for providing the feline eye specimen and Mr. John Alford for providing the CCD camera. This project is sponsored by National Institutes of Health grant R01 CA092415. Jun Ai's email is Jun8Ai@yahoo.CA. L. V. Wang's email address is LWang@oilab.tamu.edu.

References

1. G. Häusler and M. W. Lindner, "Coherence radar and spectral radar—new tools for dermatological diagnosis," J. Biomed. Opt. 3, 21–31 (1998).
2. S. H. Yun, G. J. Tearney, B. E. Bouma, B. H. Park,J. F. de Boer, "High-speed spectral-domain optical coherence tomography at 1.3 um wavelength," Opt. Express 11, 3598-3604 (2003), http://www.opticsexpress.org/
3. E. Götzinger, M. Pircher, R. A. Leitgeb, and C. K. Hitzenberger, "High speed full range complex spectral domain optical coherence tomography," Opt. Express 13, 583-594 (2005), http://www.opticsexpress.org/
4. J. Zhang, J. S. Nelson, Z. Chen, "Removal of a mirror image and enhancement of the signal-to-noise ratio in Fourier-domain optical coherence tomography using an electro-optic phase modulator," Optics Letters 30, 147-149(2005)
5. R. A. Leitgeb, C. K. Hitzenberger, A. F. Fercher, and T. Bajraszewski, "Phase shifting algorithm to achieve high speed long depth range probing by frequency domain optical coherence tomography," Opt. Lett. 28, 2201-2003 (2003)
6. J. F. de Boer, B. Cense, B.H. Park, M. C. Pierce, G. J. Tearney, and B. E. Bouma, "Signal to noise gain of spectral domain over time domain optical coherence tomography," Opt. Lett. 28, 2067-2069 (2003).
7. R. Leitgeb, C. K. Hitzenberger,A. F. Fercher, "Performance of fourier domain vs. Time domain optical coherence tomography," Opt. Express 11, 889-894 (2003), http://www.opticsexpress.org/
8. C. Dorrer, N. Belabas, J. Likforman,M. Joffre, "Spectral resolution and sampling issues in Fourier transform spectral interferometry," Journal of the Optical Society of America B 17, 1795-1802 (2000).